

# Markov Decision Process Based Design of SWIPT Systems: Non-linear EH Circuits, Memory, and Impedance Mismatch

Nikita Shanin, Laura Cottatellucci, and Robert Schober

*Friedrich-Alexander-Universität Erlangen-Nürnberg (FAU), Germany*

## Abstract

In this paper, we study simultaneous wireless information and power transfer (SWIPT) systems employing practical non-linear energy harvester (EH) circuits. Since the voltage across the reactive elements of realistic EH circuits cannot drop or rise instantaneously, EHs have *memory* which we model with a Markov decision process (MDP). Moreover, since an analytical model that accurately models all non-linear effects and the unavoidable impedance mismatch of EHs is not tractable, we propose a learning based model for the EH circuit. We optimize the input signal distribution for maximization of the harvested power under a constraint on the minimum mutual information between transmitter (TX) and information receiver (IR). We distinguish the cases where the MDP state is known and not known at TX and IR. When the MDP state is known, the formulated optimization problem for the harvested power is convex. In contrast, if TX and IR do not know the MDP state, the resulting optimization problem is non-convex and solved via alternating optimization, which is shown to yield a stationary point of the problem. Our simulation results reveal that the rate-power region of the considered SWIPT system depends on the symbol duration, the EH input power level, the EH impedance mismatch, and the type of EH circuit. In particular, a shorter symbol duration enables higher bit rates at the expense of a significant decrease in the average harvested power. Furthermore, whereas half-wave rectifiers outperform full-wave rectifiers in the low and medium input power regimes, full-wave rectifiers are preferable if the input power at the EH is high.

This work will be partially presented at the IEEE International Conference on Communications (ICC), Dublin, Ireland, 2020 [1].

## I. INTRODUCTION

The Internet-of-Things (IoT) and the related tremendous growth of the number of low-power devices have attracted significant attention in recent years. Nevertheless, the problem of the efficient recharging or replacement of the batteries of billions of IoT devices, such as wireless sensors and actuators, remains unsolved [2]. A promising exploitable feature to address this problem is the ability of radio frequency (RF) signals to transfer not only information but also energy, which can be harvested by these devices. This prospect has fueled significant interest in simultaneous wireless information and power transfer (SWIPT) systems [1]–[12].

SWIPT was studied first in [3]. The author showed that there exists a fundamental trade-off between the achievable information rate and the transferred power in discrete-time memoryless Gaussian channels. This trade-off is characterized by a non-increasing concave capacity-energy function. In [4], the authors showed that, in a frequency-selective channel with additive white Gaussian noise (AWGN), a simple sinusoidal signal is optimal for power transfer, whereas the waterfilling strategy is optimal for information transmission. In [5], a multiple-antenna SWIPT system with time switching transmission was considered. In particular, the authors proposed a protocol, where each transmission block is divided into two time slots, one for information transmission and the other one for power transfer. Additionally, in [5], two fundamental SWIPT system architectures were proposed. Specifically, the authors considered SWIPT systems, where the energy harvester (EH) and information receiver (IR) were implemented as separate devices and co-located in the same device, respectively.

An essential prerequisite for the design of a SWIPT system is to accurately model the EH circuit which is employed to convert the received RF signal to a direct current (DC) signal. An EH circuit typically includes a rectenna, i.e., an antenna followed by a rectifier. In [3]–[5], the authors assumed a linear relationship between the harvested power and the received RF power. However, recently, practical non-linear models for EH circuits were proposed for the optimization of SWIPT systems [6], [7], [9]–[12]. In [6], the author investigated a non-linear diode model obtained by a Taylor series approximation of the current flowing through the rectifier diode and showed that, for multi-carrier transmission, different input signal distributions maximize the information rate and the transferred energy. By varying the input distribution, different points in the corresponding rate-energy region can be achieved. In [7], the authors considered a rectenna circuit comprising a single diode for signal rectification, developed a non-linear diode model for

this circuit, and characterized the corresponding rate-energy region by optimally designing the input distribution to maximize the mutual information between the transmitter (TX) and the IR under a constraint on the minimum harvested power. The analysis in [7] showed that the harvested power is maximized by allocating non-zero probabilities to two mass points which correspond to the maximum and minimum transmit power values and satisfy the peak power (PP) and average power (AP) constraints of the TX. This result was supported by the experiments in [8] which showed that signals with high peak-to-average power ratio (PAPR) yield higher harvested powers compared to constant-envelope signals. Furthermore, since for high input powers, typical EH circuits are driven into saturation by the diode breakdown effect, see, e.g., [9, Figure 3], in [10], a non-linear EH model based on a parameterized sigmoid function was proposed. The authors obtained the parameters by fitting the sigmoid function to experimental data. Finally, in [11] and [12], based on the concept of autoencoder [13], the authors used a learning approach to optimize the modulation scheme to determine the trade-off between the symbol error rate for data transmission and the harvested power. In [11], the design of the modulation scheme was based on the EH model in [7], whereas in [12], the authors utilized two different EH circuit models, one similar to the model in [6] and one based on the model in [10], for low and high EH input powers, respectively. Similarly to [7], the results in [12] suggest that on-off signaling is optimal for power transfer.

Although the non-linear EH models considered in [6], [7], [9]–[12] constitute a significant progress compared to the linear model in [3]–[5], they are still based on strong assumptions. First, it is assumed that the instantaneous harvested power depends on the currently received signal only. However, rectifier circuits typically include a reactive element, usually a capacitor, as part of a low-pass filter (LPF). Since the voltage (or current) level on this element cannot drop instantaneously [14], rectenna circuits have *memory*. Furthermore, for high RF signal powers, EHs suffer from the diode breakdown effect which was only partially included in [7], [9], [10], [12] and completely neglected in [6], [11]. Moreover, the impedance values of the antenna and the rectifier have to be properly matched by a matching circuit (MC) in order to maximize the efficiency of the EH. This MC was assumed to be ideal in [6], [7], [9]–[12]. However, because of the rectifier non-linearity, perfect matching is possible for a single input signal frequency and a single power value only. Finally, in [6], [7], [9]–[12], the authors considered a rectenna circuit that comprised a single diode for half-wave signal rectification. However, other rectifier circuits may be beneficial for SWIPT system design, e.g., the full-wave rectifier based on a

bridge configuration with multiple diodes has been shown to lead to smaller output ripple [15] and higher diode breakdown voltage levels [14].

In this paper, we develop an analytical framework for SWIPT system design and maximization of the rate-power region by optimization of the input signal distribution taking into account the above mentioned effects that were ignored in previous works. The main contributions of this paper can be summarized as follows. Since the behavior of an electrical circuit is determined by the initial state of its reactive elements and the input signal, we model the EH circuit by a discrete-time Markov decision process (MDP) [16]. More specifically, the states, actions, and immediate reward of the MDP are given by the voltage levels across the load resistor of the EH circuit, the input signal received at the EH, and the amount of power harvested during a state transition, respectively. Based on this model, we first assume that the TX and IR of the SWIPT system have perfect knowledge of the instantaneous EH state. For this case, we optimize the input signal distribution for maximization of the harvested power under constraints on the minimum mutual information between TX and IR and the maximum AP and PP at the TX. The boundary of the corresponding rate-power region can be obtained by solving the resulting convex optimization problem repeatedly for different values of the required minimum mutual information. Although, in practice, it may be difficult for TX and IR to track the EH state, the obtained boundary constitutes a performance upper bound for SWIPT systems where this is not possible. Then, we drop the assumption regarding the knowledge of the EH state and formulate a new optimization problem to determine the rate-power region for this case. This new optimization problem is non-convex and we exploit alternating optimization [17]–[19] to develop a low-complexity algorithm which is guaranteed to find a stationary point of the problem. Furthermore, since an analytical model for the EH circuit that includes all non-linear effects of the rectifier and impedance mismatch is not tractable, we propose a learning based approach to deal with the non-idealities of the EH circuit. In particular, we utilize dense neural networks (DNNs) to estimate the state transition probabilities and the immediate reward of the MDP. Our simulation results reveal that knowledge of the EH state at TX and IR can improve SWIPT system performance. Moreover, our results show that the optimal input distribution and the rate-power region depend on the symbol duration, the EH impedance mismatch, the EH input signal power, and the type of rectifier circuit. In particular, a shorter symbol duration increases the achievable bit rate at the expense of a decrease of the average harvested power. Furthermore, the half-wave rectifier is shown to yield a larger rate-power region in the low and medium input

power regimes, whereas the full-wave rectifier is beneficial if the input power level at the EH is high.

Different from our preliminary work in [1], in this paper, we consider the following aspects. First, to model the EH, we generalize the Markov reward chain in [1] to an MDP based approach which allows the investigation of the role played by the EH state knowledge at TX and IR. Second, we extend the analysis from real-valued to complex-valued symbol constellations and show that, for the optimal input distribution, the phase and amplitude of the transmit signal are mutually independent and the phase is uniformly distributed. Third, besides EHs with half-wave rectifiers as in [1], we also consider EHs employing full-wave rectifiers in bridge diode configuration and MCs tuned for different input power levels.

The rest of the paper is organized as follows. In Section II, we introduce the system model, propose the MDP model for the EH, and discuss the information transmission to the IR. In Section III, to determine the boundary of the rate-power region of the considered SWIPT system, we formulate two optimization problems for the cases where both TX and IR know and do not know the instantaneous EH state, respectively. In Section IV, we provide simulation results for performance evaluation. Finally, in Section V, we draw some conclusions.

Throughout this paper, we use the following notations. Bold lower case letters stand for vectors, i.e.,  $\mathbf{x}$  is a vector, and its  $i^{\text{th}}$  element is denoted by  $x_i$ . Bold upper case letters represent matrices, i.e.,  $\mathbf{X}$  is a matrix and  $X_{i,j}$  is its element in the  $i^{\text{th}}$  row and  $j^{\text{th}}$  column. The average value of random variable (RV)  $x$  is denoted by  $\bar{x}$ .  $f(x, y; z)$  denotes a function of variables  $x$  and  $y$  for a given parameter  $z$ . The indicator function  $\mathbf{1}_X(x)$  takes value 1 if  $x$  is in set  $X$  and 0, otherwise.  $\mathbb{E}_x\{\cdot\}$  denotes the expectation with respect to the distribution of RV  $x$ . Operator  $\Re\{\cdot\}$  denotes the real part of a complex number. The Moore-Penrose pseudoinverse of a matrix is denoted by  $(\cdot)^\dagger$ .  $\mathbb{R}$  and  $\mathbb{C}$  indicate the sets of real and complex numbers, respectively. The imaginary unit is denoted by  $j$ . The circularly-symmetric complex Gaussian distribution with mean vector  $\boldsymbol{\mu}$  and covariance matrix  $\boldsymbol{\Gamma}$  is denoted by  $\mathcal{CN}(\boldsymbol{\mu}, \boldsymbol{\Gamma})$ .  $\Pr\{x = x_i\}$  stands for the probability that RV  $x$  is equal to a particular value  $x_i$ .

## II. SYSTEM MODEL AND PRELIMINARIES

In this section, first, we present the considered SWIPT system model. Then, we model the EH by an MDP and discuss the information transmission to the IR.

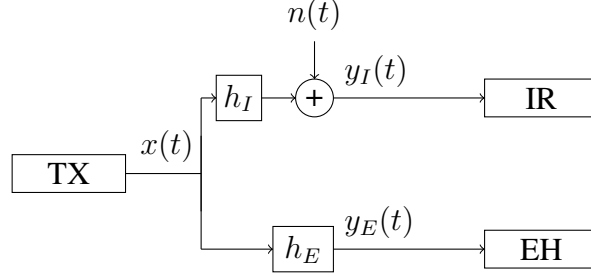


Fig. 1. SWIPT system model comprising a TX, an IR, and an EH.

### A. System Model

Let us consider the single-antenna SWIPT system shown in Fig. 1. It consists of a TX, an IR, and an EH. The TX broadcasts a pulse-modulated signal, which is modeled as  $x(t) = \sum_{k=0}^{\infty} x[k]\psi(t-kT)$ , where  $T$  is the symbol duration,  $\psi(t)$  is a rectangular transmit pulse shape, and  $x[k] \in \mathbb{C}$  is the information symbol transmitted in time slot  $k$ .

The complex-valued information symbol  $x[k]$ ,  $k \in \{0, 1, \dots\}$ , is expressed in polar coordinates as  $x[k] = r_x[k]e^{j\phi_x[k]}$ , where the amplitude  $r_x[k] \geq 0$  is a realization of an independent and identically distributed (i.i.d.) RV  $r_x$ , whereas the phase  $\phi_x[k] \in [-\pi, \pi)$  is a realization of an i.i.d. RV  $\phi_x$ . We denote the joint probability density function (pdf) of RVs  $r_x$  and  $\phi_x$  by  $p_{r_x, \phi_x}(r, \phi)$ . The complex-valued fading gains of the IR and EH channels are assumed to be constant and given by  $h_I = |h_I|e^{j\phi_I}$  and  $h_E = |h_E|e^{j\phi_E}$ , respectively. We assume that the TX has perfect knowledge of both channel gains and, additionally,  $h_I$  is known at the IR. The RF signals received at the IR and the EH can be expressed as  $y_I^{RF}(t) = \sqrt{2}\Re\{[h_I x(t) + n(t)]e^{j2\pi f_c t}\}$  and  $y_E^{RF}(t) = \sqrt{2}\Re\{h_E x(t) e^{j2\pi f_c t}\}$ , respectively, where  $f_c$  and  $n(t)$  denote the carrier frequency and complex-valued zero-mean AWGN, respectively. We note that the noise received at the EH is ignored because its contribution to the harvested energy is negligible.

### B. MDP Model of EH

In this section, we develop an MDP model for the EH. An MDP consists of a finite state space of size  $S_{\Xi}$ ,  $\Xi = \{\xi_1, \xi_2, \dots, \xi_{S_{\Xi}}\}$ , a set of actions,  $\mathcal{X}_E$ , transition probabilities, and a reward function. In particular, the current MDP state  $\xi[k] \in \Xi$  depends on the previous state  $\xi[k-1] \in \Xi$  and action  $x_E[k] \in \mathcal{X}_E$  only. Moreover, the transition from state  $\xi_i \in \Xi$  to state  $\xi_j \in \Xi$  due to

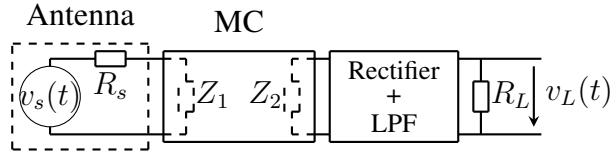


Fig. 2. EH circuit model comprising an antenna, an MC, a rectifier with an LPF, and a load resistor  $R_L$ .

action  $x_E$  occurs with transition probability  $\hat{\rho}_{i,j}(x_E)$ , and, during this transition, an immediate reward  $\hat{P}_{i,j}(x_E)$  is received.

In the following, first, we present the rectenna circuit employed by the EH. Then, we provide the MDP model for the EH. Finally, we derive an expression for the average power harvested by the EH which represents the average reward of the MDP.

1) *EH Circuit*: Similar to [2], [7], and references therein, we assume that the EH is equipped with a non-linear rectenna circuit comprising an antenna, an MC, a rectifier with an LPF, and a load resistor, cf. Fig. 2. The antenna is modeled as a voltage source  $v_s(t)$  connected in series with resistance  $R_s$ . The rectifier circuit typically includes a non-linear diode circuit and an LPF to convert the RF signal received at the EH to a low frequency output voltage  $v_L(t)$  across the load resistance  $R_L$ . Finally, as in [7] and [20], the EH includes an impedance MC, which matches the antenna output impedance  $Z_1$  and the input impedance of the rectifier circuit  $Z_2$  to maximize the power transferred from the antenna to the rectifier. Note that since the rectifier circuit includes non-linear elements, typically diodes, exact matching is possible for one frequency and one power value of the received signal only. Examples for the employed rectifiers and MCs will be provided in Section III-E.

Since the output voltage of the rectenna circuit  $v_L(t)$  is always bounded above due to the diode breakdown effect [21], we define the maximum load voltage level as  $V_L^{\max}$ . We introduce a finite set of *voltage levels* of size  $S_{\Xi} + 1$ , whose elements are defined as  $\hat{v}_l = \frac{V_L^{\max}}{S_{\Xi}}l$ ,  $l \in \{0, 1, \dots, S_{\Xi}\}$ . Furthermore, we define the set of *quantized load voltage levels* of size  $S_{\Xi}$ , whose elements are given by  $\tilde{v}_i = \frac{\hat{v}_{i-1} + \hat{v}_i}{2}$ ,  $i \in \{1, 2, \dots, S_{\Xi}\}$ . We approximate the output voltage level  $v_L(t)$  by discrete value  $\tilde{v}_i$  if  $v_L(t) \in [\hat{v}_{i-1}, \hat{v}_i)$ . Note that if the number of quantization levels approaches infinity, i.e.,  $S_{\Xi} \rightarrow \infty$ , then  $\tilde{v}(t) \rightarrow v_L(t)$ .

2) *EH States*: In the following, we model the EH as an MDP. For the proposed model, we treat the quantized voltage levels at the load resistor,  $\tilde{v}_l, l \in \{1, 2, \dots, S_{\Xi}\}$ , and the received symbols

at the EH,  $x_E[k] = h_E x[k]$ , as the states<sup>1</sup> and actions of the MDP, respectively. Furthermore, we approximate the amount of power harvested during the transition from the previous EH state  $\xi$  to the current state due to received symbol  $x_E$  by the immediate reward function  $P(\xi, x_E)$ .

More in detail, we map the discrete voltage levels  $\tilde{v}$  to the EH states  $\xi \in \Xi$  of a stochastic process, where  $\Xi \subset \mathbb{R}^{S_\Xi}$  is a finite state space. We note that, since the received RF signal  $y_E^{RF}(t)$  is time-slotted, so is the output voltage signal  $v_L(t)$ . Thus, the system is in state  $\xi[k] = \xi_i \in \Xi$ , if at time instant  $t = kT$ , the load voltage level  $v_L(kT) \in [\hat{v}_{i-1}, \hat{v}_i)$ , such that it is approximated by the quantized voltage level  $\tilde{v}(kT)$  associated with this state, i.e.,  $\xi[k] = \xi_i = \tilde{v}_i = \tilde{v}(kT)$ . Moreover, due to the memory introduced by the LPF, at the end of time interval  $k$ , the attained value  $v_L(kT)$  of the load voltage level depends on the received symbol  $x_E[k] = h_E x[k]$  and the load voltage level at the end of the previous time interval,  $v_L((k-1)T)$ . We note that although the MC typically includes additional reactive elements, it is designed as a band-pass filter for the received signal and fine-tuned to carrier frequency  $f_c$ . Furthermore, the bandwidth of this filter is much larger than the symbol rate  $\frac{1}{T}$ . Therefore, the memory introduced by the MC to the energy harvesting process is negligible, and thus, we do not include the reactive elements of the MC in our MDP model.

Stochastic process  $\{\xi[k]\}$  may change its value in each symbol interval, i.e., when the EH receives a new symbol. Therefore,  $\{\xi[k]\}$  is a discrete-time process and its *time step* is equal to the symbol duration. Thus, since the behavior of the EH circuit in a given time interval is completely determined by the initial conditions and the input signal [14],  $\xi[k]$  depends only on the voltage level of the load resistance at time  $(k-1)T$ , i.e., the previous state  $\xi[k-1]$ , and the received symbol  $x_E[k]$ . Hence, the symbol  $x_E[k]$  received at the EH corresponds to an action of the MDP that is taken in time step  $k$ , i.e., when the MDP transits from state  $\xi[k-1]$  to state  $\xi[k]$ . Thus, the probability of any state of the stochastic process  $\xi[k]$  depends only on the previous state  $\xi[k-1]$  and the received symbol  $x_E[k]$ , i.e.,  $\Pr\{\xi[k] \mid x_E[k], \xi[k-1], x_E[k-1], \xi[k-2], \dots, x_E[1], \xi[0]\} = \Pr\{\xi[k] \mid x_E[k], \xi[k-1]\}$ . Furthermore, we note that, for the considered narrowband signals, the symbol duration is typically much larger than the period of the RF signal, i.e.,  $T \gg \frac{1}{f_c}$ . Moreover, the time constant of the LPF is typically also much

<sup>1</sup>Note that, in this paper, we assume that the EH circuit comprises a first-order LPF which includes a single reactive element, namely, a capacitor. This leads to a one-dimensional MDP state space,  $\Xi$ . The extension of the proposed approach to higher order LPFs with multiple reactive elements is relatively straightforward and can be accomplished by increasing the number of dimensions of the MDP state space, see e.g. [22].



larger than  $\frac{1}{f_c}$ . Hence, we assume that the rectifier behaves as an envelope detector [23], and hence, neglect the influence of the phase changes from one received symbol to the next one on the harvested power. Therefore, the state  $\xi$  is independent of the phase  $\phi_{x_E} = \phi_x + \phi_E$  of the received signal and depends on its amplitude  $r_E = |h_E|r_x$  only. Moreover, since channel gain  $h_E$  is assumed to be perfectly known at the TX,  $\Pr\{\xi[k] \mid r_x[k], \xi[k-1]\} = \Pr\{\xi[k] \mid x_E[k], \xi[k-1]\}$  and, thus, the sequence of pairs  $\{\xi, r_x\}$  can be modeled as an MDP [24], [25].

We denote the probability of transition from state  $\xi_i \in \Xi$  to state  $\xi_j \in \Xi$  when a symbol with amplitude  $r_x$  is transmitted by  $\rho_{i,j}(r_x) = \Pr\{\xi_j \mid r_x, \xi_i\}$ . Next, we note that, for a given  $v_L((k-1)T) = v_\nu$ , the reception of a symbol with amplitude  $r_E = |h_E|r_x$  determines the output voltage level in the next time slot,  $v_L(kT) = v_\mu$ . Then,  $\Pr\{v_\mu \mid r_E, v_\nu\}$  is equal to 1 if the reception of a symbol with amplitude  $r_E$  leads to the transition from  $v_\nu$  to  $v_\mu$  and 0, otherwise. Thus,  $v_\mu$  can be obtained as a deterministic function of  $r_E$  and  $v_\nu$ , i.e.,  $v_\mu = f_v(v_\nu, r_E)$ . However, since the states  $\xi_i$  and  $\xi_j$  comprise voltage levels from the intervals  $\hat{V}_i = [\hat{v}_{i-1}, \hat{v}_i)$  and  $\hat{V}_j = [\hat{v}_{j-1}, \hat{v}_j)$ , respectively, the transition probabilities of the discrete MDP  $\rho_{i,j}(r_x)$  may take any value from the interval  $[0, 1]$  and can be calculated as follows

$$\rho_{i,j}(r_x) = \frac{\int_{\hat{V}_i} \mathbf{1}_{\hat{V}_j}(f_v(v, |h_E|r_x)) dv}{\hat{v}_i - \hat{v}_{i-1}}. \quad (1)$$

We note that an analytical evaluation of  $\rho_{i,j}(r_x)$  is intractable since the transition function  $f_v(v_\nu, r_E)$  cannot be derived analytically due to the rectifier non-linearity, the imperfections of the MC, and the circuit memory. Therefore, in Section III-E, we employ a DNN [13] to approximate  $f_v(v_\nu, r_E)$  and, thus, to compute the transition probabilities  $\rho_{i,j}(r_x)$ .

Finally, we assume that the MDP is ergodic, i.e., for a given input signal distribution, starting from any initial state, the MDP always reaches the same steady-state distribution [24]. Then, we denote the joint pdf of state  $\xi_i \in \Xi$  and symbol amplitude  $r_x$  by  $\pi_i(r_x)$  and collect these pdfs in vector  $\boldsymbol{\pi}(r_x) \in \mathbb{R}^{S_\Xi}$ , which is a solution of the following system of balance equations [16]

$$\sum_{i=1}^{S_\Xi} \int_{r_x} \pi_i(r_x) (\mathbf{1}_j(i) - \rho_{i,j}(r_x)) dr_x = 0, \quad \forall j \in \{1, 2, \dots, S_\Xi\}, \quad (2)$$

$$\sum_{i=1}^{S_\Xi} \int_{r_x} \pi_i(r_x) dr_x = 1. \quad (3)$$

3) *MDP Reward*: In the following, we derive an expression for the average harvested power which constitutes the average reward of the MDP.

First, we note that the instantaneous harvested power can be expressed as  $P(t) = \frac{v_L^2(t)}{R_L}$  and, thus, similarly to  $v_L(t)$ ,  $P(t)$  is a time-slotted random process. We denote the average power harvested while receiving an infinitely long sequence of random symbols  $\{x_E[k]\}$  by  $\bar{P}$ . This value can be estimated by averaging function  $P(t)$  over time, or equivalently, over time intervals, assuming that the number of time intervals  $K$  approaches infinity:

$$\bar{P} = \lim_{t \rightarrow \infty} \frac{1}{t} \int_0^t P(\tau) d\tau = \lim_{K \rightarrow \infty} \frac{1}{K} \sum_{k=0}^{K-1} \frac{1}{T} \int_0^T P(t + kT) dt. \quad (4)$$

Since the amount of power harvested by the EH during time slot  $k$  depends on the amplitude  $r_E = |h_E|r_x$  of the symbol received in time slot  $k$  and on the load voltage level at the end of the previous time slot  $v_\mu = v_L((k-1)T)$ , we define the harvested power averaged over symbol duration  $T$  by  $P'(v_\mu, r_E) = \frac{1}{T} \int_0^T P(t + (k-1)T) dt$ . Furthermore, the average amount of power,  $\tilde{P}_i(r_x)$ , harvested if the previous state is  $\xi[k-1] = \xi_i \in \Xi$  and a symbol with amplitude  $r_E = |h_E|r_x$  is received, is approximated as  $\tilde{P}_i(r_x) = P'(\tilde{v}_i, |h_E|r_x)$ . Additionally, since the MDP is assumed to be ergodic, the influence of the initial state on the average harvested power vanishes as the length of the symbol sequence  $\{x[k]\}, k = \{0, 1, 2, \dots\}$ , increases. Hence, the average harvested power can be obtained as a function of  $\boldsymbol{\pi}(r_x)$  by averaging  $\tilde{P}_i(r_x)$  over both the EH states and the transmitted symbols as follows

$$\bar{P}(\boldsymbol{\pi}(r_x)) = \mathbb{E}_{\xi, r_x} \{ \tilde{P}_i(r_x) \} = \sum_{i=1}^{S_\Xi} \int_{r_x} \pi_i(r_x) \tilde{P}_i(r_x) dr_x. \quad (5)$$

Since  $P'(v, r_E)$  is also not analytically tractable, in Section III-E, we employ a second DNN to approximate this function.

### C. Information Receiver

Let us consider the signal received at the IR,  $y_I^{RF}(t)$ . Since  $y_I^{RF}(t)$  is a time-slotted signal, after down-conversion, matched filtering, and sampling, the received signal in time slot  $k$  can be expressed as  $y[k] = h_I x[k] + n[k]$ , where  $n[k]$  is discrete-time AWGN distributed as  $\mathcal{CN}(0, 2\sigma_n^2)$ . Furthermore,  $y[k]$  can be expressed in polar coordinates as  $y[k] = r_y[k] e^{j\phi_y[k]}$  with  $r_y[k] \geq 0$  and  $\phi_y[k] \in [-\pi, \pi)$ , where amplitude  $r_y[k]$  and phase  $\phi_y[k]$  are realizations of i.i.d. RVs  $r_y$  and  $\phi_y$ , respectively. We denote the joint pdf of RVs  $r_y$  and  $\phi_y$  as a function of the joint input pdf  $p_{r_x, \phi_x}$  by  $p_{r_y, \phi_y}(r, \phi; p_{r_x, \phi_x})$ .

The mutual information between  $x$  and  $y$  as a function of the joint input pdf  $p_{r_x, \phi_x}(r, \phi)$  can be expressed as [26]

$$I(p_{r_x, \phi_x}) = H_y(p_{r_x, \phi_x}) - H_n, \quad (6)$$

where  $H_y(p_{r_x, \phi_x})$  and  $H_n$  are the differential entropies of the received signal and the noise, respectively. We note that the differential entropy of the noise does not depend on the input pdf  $p_{r_x, \phi_x}(r, \phi)$  and is equal to  $H_n = \log_2(2\pi e\sigma_n^2)$  [27]. The differential entropy of the complex-valued received signal can be expressed as follows [28]

$$H_y(p_{r_x, \phi_x}) = H_{r_y, \phi_y}(p_{r_x, \phi_x}) + \int_0^\infty p_{r_y}(r; p_{r_x, \phi_x}) \log_2(r) dr, \quad (7)$$

where  $p_{r_y}(r; p_{r_x, \phi_x})$  and  $H_{r_y, \phi_y}(p_{r_x, \phi_x})$  denote the pdf of RV  $r_y$  and the differential entropy of RVs  $r_y$  and  $\phi_y$  as functions of input pdf  $p_{r_x, \phi_x}$ , respectively.

### III. RATE-POWER REGION OF SWIPT SYSTEM

We refer to the set of all attainable pairs of average harvested powers and achievable rates as the rate-power region of the SWIPT system [7]. In order to obtain the boundary of this rate-power region, in this section, we jointly optimize the pdfs of the EH states  $\xi$ , transmit symbol amplitudes  $r_x$ , and transmit symbol phases  $\phi_x$  for maximization of the harvested power at the EH under a constraint on the minimum required mutual information between TX and IR. To this end, we first consider the case where both TX and IR have perfect knowledge of the instantaneous EH state which leads to a convex optimization problem. Then, we consider the more practical case, where the EH state is not known at TX and IR. In this case, the resulting optimization problem is non-convex, and we develop an iterative algorithm to obtain a stationary point [19].

#### A. EH State Is Known at TX and IR

In this section, we assume that both TX and IR know the current EH state. This assumption may hold in practice if, e.g., the IR and EH are co-located devices [2] and the TX is able to track the EH state. Under this assumption, the pdf of the transmit symbols, which must be known at TX and IR, can be made dependent on the EH state  $\xi$  and, hence, be modeled as  $p_{r_x, \phi_x}^i = p_{r_x}^i p_{\phi_x|r_x}^i$ , where subscript  $i$  refers to the pdf for EH state  $\xi_i$  and  $p_{\phi_x|r_x}^i$  is the conditional pdf of phase  $\phi_x$  for a given amplitude  $r_x$ . Thus, we obtain the boundary of the rate-power region by jointly optimizing the joint pdf of the EH states  $\xi$  and the amplitudes  $r_x$  of transmitted symbol  $x$ ,  $\pi(r_x)$ , and the set of conditional pdfs  $\mathcal{P}_{\phi_x|r_x}$ , whose  $i^{\text{th}}$  element is  $\mathcal{P}_{\phi_x|r_x}^i = p_{\phi_x|r_x}^i$ ,  $i \in \{1, 2, \dots, S_\Xi\}$ .

We note that, for a given joint pdf  $\boldsymbol{\pi}(r_x)$ , the pdf of the symbol amplitudes in state  $\xi_i$  is given by [16]

$$p_{r_x}^i(r) = \frac{\pi_i(r)}{\gamma_i}, \quad (8)$$

where  $\gamma_i = \int_{r_x} \pi_i(r_x) dr_x$  denotes the marginal probability of state  $\xi_i \in \Xi$ . Additionally, since in each symbol interval  $k$ , transmitted symbol  $x[k]$  may be taken from a different distribution depending on the current EH state, we introduce the *expected mutual information* averaged over the EH states, which is given by  $\bar{I}(\boldsymbol{\pi}(r_x), \mathcal{P}_{\phi_x|r_x}) = \sum_{i=1}^{S_\Xi} \gamma_i I(p_{r_x, \phi_x}^i)$ . Hence, we formulate the following constrained optimization problem

$$\underset{\boldsymbol{\pi}(r_x), \mathcal{P}_{\phi_x|r_x}}{\text{maximize}} \quad \bar{P}(\boldsymbol{\pi}(r_x)) \quad (9a)$$

$$\text{subject to} \quad \bar{I}(\boldsymbol{\pi}(r_x), \mathcal{P}_{\phi_x|r_x}) \geq I_{\text{req}}, \quad (9b)$$

$$\sum_{i=1}^{S_\Xi} \int_{r_x} r_x^2 \pi_i(r_x) dr_x \leq \sigma_{r_x}^2, \quad (9c)$$

$$|r_x| \leq r_x^{\text{max}}, \quad (9d)$$

$$\sum_{i=1}^{S_\Xi} \int_{r_x} \pi_i(r_x) dr_x = 1, \quad (9e)$$

$$\sum_{i=1}^{S_\Xi} \int_{r_x} \pi_i(r_x) (\mathbf{1}_j(i) - \rho_{i,j}(r_x)) dr_x = 0, \quad j \in \{1, 2, \dots, S_\Xi\}, \quad (9f)$$

where  $I_{\text{req}}$  in (9b) is the minimum required expected mutual information between TX and IR. Constraint (9c) limits the AP budget at the TX to  $\sigma_{r_x}^2$  to avoid excessive power consumption and interference to other systems. Moreover, to avoid driving the power amplifier into a non-linear regime, we impose constraint (9d) to limit the PP at the TX by introducing the maximum amplitude  $r_x^{\text{max}}$ . Furthermore, constraints (9e) and (9f) ensure that the solution  $\boldsymbol{\pi}(r_x)$  is a valid pdf, i.e., summing the probabilities over the MDP state and action spaces yields one, and corresponds to the steady-state distribution of the MDP described in Section II-B, respectively.

Note that since  $\boldsymbol{\pi}(r_x)$  is independent of  $\phi_x$ , in (9), only  $\bar{I}(\boldsymbol{\pi}(r_x), \mathcal{P}_{\phi_x|r_x})$  depends on the distribution of the phases  $\phi_x$ . In the following proposition, we show that for the solution of (9), the individual phase distributions in  $\mathcal{P}_{\phi_x|r_x}$  are independent of EH state  $\xi$ , i.e.,  $p_{\phi_x|r_x}^1 = p_{\phi_x|r_x}^2 = \dots = p_{\phi_x|r_x}^{S_\Xi}$ , and the phases  $\phi_x$  are statistically independent of the symbol amplitude  $r_x$  and uniformly distributed.

**Proposition 1.** *For the solution of (9), the phase  $\phi_x$  of transmitted symbol  $x = r_x e^{j\phi_x}$  is uniformly distributed and statistically independent from amplitude  $r_x$  and EH state  $\xi$ . Moreover, RVs  $r_y$  and  $\phi_y$  are also statistically independent and phase  $\phi_y$  is uniformly distributed. Furthermore, the mutual information and the distribution of the amplitudes of the received symbol, when the EH is in state  $\xi_i$ , can be simplified as follows*

$$I(p_{r_x, \phi_x}^i) = I(p_{r_x}^i) = - \int_0^\infty p_{r_y}(r_y; p_{r_x}^i) \log_2 \left( \frac{1}{r_y} p_{r_y}(r_y; p_{r_x}^i) \right) dr_y + \log_2(2\pi) - H_n, \quad (10)$$

$$p_{r_y}(r_y; p_{r_x}^i) = \frac{1}{\sigma_n^2} \int_{r_x} r_y e^{-\frac{r_y^2 + r_x^2 |h_I|^2}{2\sigma_n^2}} I_0 \left( \frac{r_y r_x |h_I|}{\sigma_n^2} \right) p_{r_x}^i(r_x) dr_x. \quad (11)$$

*Proof.* Please refer to Appendix A. ■

Exploiting Proposition 1, we can reformulate the constrained optimization problem in (9) as follows

$$\underset{\pi(r_x)}{\text{maximize}} \quad \bar{P}(\pi(r_x)) \quad (12a)$$

$$\text{subject to} \quad \bar{I}(\pi(r_x)) = \sum_{i=1}^{S_\Xi} \gamma_i I(p_{r_x}^i) \geq I_{\text{req}}, \quad (12b)$$

(9c)-(9f),

where the pdf of the symbol amplitudes,  $p_{r_x}^i(r)$ , is calculated as in (8).

The solution of (12),  $\pi^*(r_x)$ , is the optimal joint pdf of the EH states and the transmitted symbols and maximizes the average harvested power at the EH subject to the constraints on the expected mutual information between TX and IR, the AP, and the PP at the TX. Optimization problem (12) is convex and, hence, can be efficiently solved using standard numerical tools, such as CVX [29].

To implement the policy obtained by solving (12), the input distribution has to be adapted at the TX according to the instantaneous EH state, i.e., TX and IR must have perfect knowledge of the current EH state. This may be difficult to realize in practice. Nevertheless,  $\pi^*(r_x)$  constitutes a performance upper-bound for the more practical case where the EH state is not known at TX and IR. The rate-power region for this case will be tackled next.

### B. EH State Is Not Known at TX and IR

Now, we consider SWIPT systems where the current EH state is not known at TX and IR. Tracking the EH state increases complexity and may not be possible when EH and IR are separated.

If the EH state is not known, the pdf of the input symbol amplitudes,  $p_{r_x}$ , which must be known at both TX and IR, has to be independent of  $\xi$ , i.e.,  $p_{r_x}^i(r) = p_{r_x}(r)$ ,  $\forall i \in \{1, 2, \dots, S_\Xi\}$ . Then, the joint pdf  $\pi(r_x)$  and the average harvested power,  $\bar{P}$ , reduce as follows

$$\pi_i(r_x) = \gamma_i p_{r_x}(r_x), \quad (13)$$

$$\bar{P}(\gamma, p_{r_x}) = \sum_{i=1}^{S_\Xi} \int_{r_x} \gamma_i p_{r_x}(r_x) \tilde{P}_i(r_x) dr_x, \quad (14)$$

where vector  $\gamma = [\gamma_1, \gamma_2, \dots, \gamma_{S_\Xi}]^\top$  collects the marginal probabilities of the EH states  $\xi_i$ ,  $i \in \{1, 2, \dots, S_\Xi\}$ . In order to obtain the boundary of the rate-power region, we formulate the following optimization problem:

$$\underset{\gamma, p_{r_x}}{\text{maximize}} \quad \bar{P}(\gamma, p_{r_x}) \quad (15a)$$

$$\text{subject to} \quad I(p_{r_x}) \geq I_{\text{req}}, \quad (15b)$$

$$\int_{r_x} r_x^2 p_{r_x}(r_x) dr_x \leq \sigma_{r_x}^2, \quad (15c)$$

$$|r_x| \leq r_x^{\text{max}}, \quad (15d)$$

$$\sum_{i=1}^{S_\Xi} \int_{r_x} \gamma_i p_{r_x}(r_x) (\mathbf{1}_j(i) - \rho_{i,j}(r_x)) dr_x = 0, \quad j \in \{1, 2, \dots, S_\Xi\}, \quad (15e)$$

$$\int_{r_x} p_{r_x}(r_x) dr_x = 1, \quad (15f)$$

$$\sum_{i=1}^{S_\Xi} \gamma_i = 1, \quad (15g)$$

where, similar to (9), we maximize the average harvested power at the EH,  $\bar{P}$ , subject to the minimum required mutual information,  $I_{\text{req}}$ , between TX and IR. Note that, in contrast to problem (9), since, in this case, the distribution  $p_{r_x}$  is identical in each symbol interval, the expected mutual information  $\bar{I}(\pi(r_x))$  is equal to the mutual information  $I(p_{r_x})$  for any given state, cf. (15b). Constraints (15c) and (15d) ensure that the input distribution  $p_{r_x}$  satisfies the AP and PP limits at the TX, respectively. Furthermore, we have reformulated constraint (9f) as (15e), whereas (9e) has been decomposed into (15f) and (15g).

We observe that objective function (15a) and constraint (15e) are not jointly concave and convex with respect to  $\gamma$  and  $p_{r_x}$ , respectively. Hence, (15) is a non-convex optimization problem, and therefore, the computation of its global optimal solution entails a high complexity. However, if we fix one of the variables, i.e.,  $\gamma$  or  $p_{r_x}$ , both (15a) and (15e) become linear in the other variable. Hence, the subproblems obtained from (15) by fixing either  $\gamma$  or  $p_{r_x}$  are convex and can be solved efficiently. Therefore, in the following, to find a suboptimal solution of (15), we adopt alternating optimization, e.g., [17], which is known for its high efficiency and fast convergence speed. The solution obtained by the proposed algorithm converges to a stationary point of (15).

### C. Algorithm for Solving (15)

In the following, we develop an iterative algorithm, which involves an inner and an outer loop, to obtain a suboptimal solution of (15). In the outer loop of the algorithm, as in [30], we relax the equality constraints in (15e) to inequality constraints and tighten the relaxation in each iteration. In the inner loop, adopting alternating optimization, we obtain a stationary point of the relaxed version of problem (15).

1) *Outer Loop:* We observe that the optimization variables in problem (15) can be separated into two non-overlapping subsets, i.e., the pdf of symbol amplitudes,  $p_{r_x}$ , and the distribution of EH states,  $\gamma$ , and therefore, alternating optimization is a promising approach for solving (15) [18]. However, (15e) imposes  $S_{\Xi}$  equality constraints. Hence, applying alternating optimization directly to (15) may lead to a strongly suboptimal solution since, in each iteration, the degrees of freedom for the optimization of  $p_{r_x}$  and  $\gamma$  are very limited. Thus, to overcome this issue, similar to [30], we first relax the equality constraints in (15e) to inequality constraints as follows

$$\left| \int_{r_x} p_{r_x}(r_x) \sum_{i=1}^{S_{\Xi}} \gamma_i (\mathbf{1}_j(i) - \rho_{i,j}(r_x)) dr_x \right| \leq \epsilon_m^{\text{tol}}, \quad j \in \{1, 2, \dots, S_{\Xi}\}, \quad (16)$$

where  $\epsilon_m^{\text{tol}} = \epsilon_{m-1}^{\text{tol}} \delta_{\epsilon}$  is the tolerance for the constraint violation, which will be tightened in each iteration of the outer loop, and  $\delta_{\epsilon} \leq 1$  is a constant factor.

Furthermore, we note that, for a given distribution of symbol amplitudes  $p_{r_x}$  which satisfies (15b) - (15d), (15f), there exists a unique distribution of EH states  $\gamma$ , such that the pair  $\{p_{r_x}, \gamma\}$  is in the feasible set of (15) [24]. This distribution of EH states,  $\gamma$ , can be obtained as the unique solution of the system of balance equations defined by constraints (15e) and (15g). Moreover, we note that (15e) and (15g) can be rewritten in matrix form as  $\mathbf{R}(p_{r_x})\gamma = \mathbf{e}$ , where the elements of  $\mathbf{R}(p_{r_x}) \in \mathbb{R}^{(S_{\Xi}+1) \times S_{\Xi}}$  are given by  $R(p_{r_x})_{j,i} = \int_{r_x} p_{r_x}(r_x) (\mathbf{1}_j(i) - \rho_{i,j}(r_x)) dr_x$  and

$R(p_{r_x})_{S_{\Xi}+1,i} = 1, i, j \in \{1, 2, \dots, S_{\Xi}\}$ , whereas the elements of  $\mathbf{e} \in \mathbb{R}^{(S_{\Xi}+1)}$  are all equal to zero, i.e.,  $e_i = 0$  if  $i \in \{1, 2, \dots, S_{\Xi}\}$ , except for the last element, which is  $e_{S_{\Xi}+1} = 1$ .

We note that one of the equations in (15e) is redundant and, hence, the rank of matrix  $\mathbf{R}(p_{r_x})$  is equal to  $S_{\Xi}$  [24]. Thus, for an initial feasible pdf of symbol amplitudes in iteration  $m$ ,  $p_{r_x}^{m,0}$ , we obtain the corresponding distribution of states  $\gamma^{m,0}$  as follows

$$\gamma^{m,0} = (\mathbf{R}(p_{r_x}^{m,0}))^{\dagger} \mathbf{e}. \quad (17)$$

Then, starting from the initial point  $\{p_{r_x}^{m,0}, \gamma^{m,0}\}$ , we find a stationary solution of problem (15) with constraint (15e) relaxed to (16),  $\{p_{r_x}^{m,*}, \gamma^{m,*}\}$ , utilizing alternating optimization, which is implemented in the inner loop of the proposed algorithm. Finally, we obtain the initial point for the next iteration  $m + 1$  from  $\{p_{r_x}^{m,*}, \gamma^{m,*}\}$  by setting  $p_{r_x}^{m+1,0} = p_{r_x}^{m,*}$  and calculating the corresponding feasible distribution of EH states,  $\gamma^{m+1,0}$ , as in (17).

2) *Inner Loop*: In the inner loop, exploiting alternating optimization, we solve the subproblem obtained in outer loop iteration  $m$  by relaxing constraint (15e) to (16). To this end, we sequentially fix one of the optimization variables, i.e.,  $\gamma$  or  $p_{r_x}$ , and solve the resulting convex subproblem with respect to the other variable.

**Step 1:** In the first step of the  $n^{\text{th}}$  iteration of the inner loop, we optimize the pdf of the symbol amplitudes  $p_{r_x}$  for the given distribution of states  $\gamma^{m,n-1}$  calculated in iteration  $n - 1$ . Since constraint (15g) does not depend on pdf  $p_{r_x}$ , in the current step, we obtain the pdf of symbol amplitudes  $p_{r_x}^{m,n}$  as solution of the following optimization subproblem

$$\begin{aligned} & \underset{p_{r_x}}{\text{maximize}} \quad \bar{P}(\gamma^{m,n-1}, p_{r_x}) & (18) \\ & \text{subject to} \quad \left| \int_{r_x} p_{r_x}(r_x) \sum_{i=1}^{S_{\Xi}} \gamma_i^{m,n-1} (\mathbf{1}_j(i) - \rho_{i,j}(r_x)) dr_x \right| \leq \epsilon_m^{\text{tol}}, \quad j \in \{1, 2, \dots, S_{\Xi}\} \\ & \quad (15b), (15c), (15d), (15f). \end{aligned}$$

**Step 2:** We note that constraints (15b), (15c), (15d), and (15f) do not depend on the distribution of states  $\gamma$ . Hence, for the given pdf  $p_{r_x}^{m,n}$ , we formulate the subproblem to obtain  $\gamma^{m,n}$  as follows

$$\begin{aligned} & \underset{\gamma}{\text{maximize}} \quad \bar{P}(\gamma, p_{r_x}^{m,n}) & (19) \\ & \text{subject to} \quad \left| \sum_{i=1}^{S_{\Xi}} \gamma_i \int_{r_x} p_{r_x}^{m,n}(r_x) (\mathbf{1}_j(i) - \rho_{i,j}(r_x)) dr_x \right| \leq \epsilon_m^{\text{tol}}, \quad j \in \{1, 2, \dots, S_{\Xi}\} \\ & \quad (15g). \end{aligned}$$



First, we note that problem (18) is convex, whereas (19) is linear and, hence, both problems can be efficiently solved using standard numerical optimization tools, such as CVX. Then, we observe that, in each iteration of the inner loop, the average harvested power increases, i.e.,  $\bar{P}(\gamma^{m,n}, p_{r_x}^{m,n}) \geq \bar{P}(\gamma^{m,n-1}, p_{r_x}^{m,n-1})$  and, hence, starting from the feasible point  $\{\gamma^{m,0}, p_{r_x}^{m,0}\}$ , the sequence  $\{\gamma^{m,n}, p_{r_x}^{m,n}\}$  converges to a stationary point of the corresponding relaxed subproblem,  $\{\gamma^{m,*}, p_{r_x}^{m,*}\}$  [17], [18]. Moreover, as outer loop iteration  $m$  increases, the feasible set of the relaxed subproblem determined by constraints (15b) - (15d), (15f), (15g), and (16) shrinks to the feasible set of the initial problem (15). Hence, assuming sufficiently large numbers of iterations in the inner loop,  $N_{\max}$ , and the outer loop,  $M_{\max}$ , the sequence of stationary points  $\{\gamma^{m,N_{\max}}, p_{r_x}^{m,N_{\max}}\} = \{\gamma^{m,*}, p_{r_x}^{m,*}\}$  converges to a stationary point of (15) denoted by  $\{\gamma^*, p_{r_x}^*\}$ . Furthermore, since the monotonicity of the sequence  $\bar{P}(\gamma^{m,0}, p_{r_x}^{m,0}), m \in \{1, 2, \dots, M_{\max}\}$ , cannot be guaranteed in general, as a suboptimal solution of (15), one may choose the pair  $\langle \gamma', p_{r_x}' \rangle = \arg \max_{\langle \gamma, p_{r_x} \rangle \in \mathcal{G}} \bar{P}(\gamma, p_{r_x})$ , where  $\mathcal{G} = \{\langle \gamma^{m,0}, p_{r_x}^{m,0} \rangle \mid m \in \{1, 2, \dots, M_{\max}\}\}$  is the set of feasible points obtained in the outer loop and  $M_{\max}$  is the maximum number of iterations of the outer loop. However, since we observed monotonic convergence in our simulations, as a solution of (15), we adopt the pair  $\{\gamma^{M_{\max}, N_{\max}}, p_{r_x}^{M_{\max}, N_{\max}}\}$ , which is a stationary point of (15) provided that  $M_{\max}$  is large enough to ensure that  $\epsilon_{M_{\max}}^{\text{tol}} \rightarrow 0$ . The proposed optimization algorithm is summarized in Algorithm 1.

#### D. Infinitely Large Symbol Duration

In the following, we consider the special case of a SWIPT system with symbol duration  $T \rightarrow \infty$ . First, in this case, we observe that the reactive element of the LPF in the EH circuit saturates to a voltage level which depends on the received symbol only [14]. Hence, the next state  $\xi[k]$  of the MDP does not depend on the previous state  $\xi[k-1]$ , i.e.,  $\Pr\{\xi[k] \mid r_x[k], \xi[k-1]\} = \Pr\{\xi[k] \mid r_x[k]\}$ . Then, the transition pdf of this process reduces to  $\rho_{i,j}(r_x) = \rho_i(r_x), \forall j \in \{1, 2, \dots, S_{\Xi}\}$ . Moreover, in this scenario, the power harvested by the EH before the voltage level at the reactive element in the LPF saturates becomes negligible as  $T \rightarrow \infty$ . Hence, the amount of power harvested by the EH during time slot  $k$  does not depend on the initial state  $\xi[k]$ , i.e.,  $\tilde{P}_i(r_x) = P'(\tilde{v}_i, |h_E|r_x) = P'(|h_E|r_x), \forall i \in \{1, 2, \dots, S_{\Xi}\}$ . Thus, the average harvested power in (5) depends on the pdf  $p_{r_x}$  only, i.e.,  $\bar{P}(\pi(r_x)) = \bar{P}(p_{r_x}) = \mathbb{E}_{r_x}\{P'(|h_E|r_x)\}$ . In this case, the average harvested power  $\bar{P}(p_{r_x}) = \int_{r_x} p_{r_x}(r_x) P'(|h_E|r_x) dr_x$  is maximized by optimizing the

---

**Algorithm 1:** Iterative algorithm for solving optimization problem (15)

---

Initialize: Maximum number of iterations  $M_{\max}$ ,  $N_{\max}$ , iteration indices  $m = 1$ ,  $n = 1$ , initial tolerance  $\epsilon_1^{\text{tol}}$ , constant factor  $\delta_\epsilon$ , and initial distribution  $p_{r_x}^{1,0}$  satisfying (15b)-(15d), (15f).

**repeat**

1. For distribution  $p_{r_x}^{m,0}$ , set the elements of  $\mathbf{R}(p_{r_x}^{m,0})$  as

$$R(p_{r_x}^{m,0})_{i,j} = \int_{r_x} p_{r_x}^{m,0}(r_x) (\mathbf{1}_j(i) - \rho_{i,j}(r_x)) dr_x \text{ and } R(p_{r_x}^{m,0})_{i,S_\Xi+1} = 1, \\ i, j \in \{1, 2, \dots, S_\Xi\}$$

2. Find the initial distribution of states  $\gamma^{m,0}$  from (17)

**repeat**

a. For the given  $\gamma^{m,n-1}$ , solve convex problem (18) and store the intermediate pdf of transmit symbol amplitudes  $p_{r_x}^{m,n}$

b. For the given  $p_{r_x}^{m,n}$ , solve convex problem (19) and store the intermediate distribution of states  $\gamma^{m,n}$

c. Set  $n = n + 1$

**until**  $n = N_{\max} + 1$ ;

3. Set initial value for the next iteration  $p_{r_x}^{m+1,0} = p_{r_x}^{m,N_{\max}}$

4. Update the constraint violation tolerance  $\epsilon_{m+1}^{\text{tol}} = \epsilon_m^{\text{tol}} \delta_\epsilon$

5. Set  $m = m + 1$

**until**  $m = M_{\max} + 1$ ;

**Output:**  $\gamma^{M_{\max}, N_{\max}}, p_{r_x}^{M_{\max}, N_{\max}}$

---

pdf of the transmitted symbols  $p_{r_x}$  which is independent of  $\xi$ , and hence, is identical in each symbol interval. Consequently, (9) simplifies as follows

$$\underset{p_{r_x}}{\text{maximize}} \bar{P}(p_{r_x}) \quad (20a)$$

$$\text{subject to } I(p_{r_x}) \geq I_{\text{req}}, \quad (20b)$$

$$\int_{r_x} p_{r_x}(r_x) dr_x = 1, \quad (20c)$$

$$(9c), (9d). \quad (20d)$$

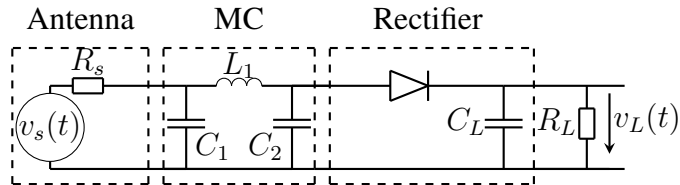


Fig. 3. EH circuit model comprising an MC, a single diode half-wave rectifier, and a capacitor  $C_L$  as part of an LPF.

We observe that optimization problem (20) is convex and can be solved using standard numerical solvers, such as CVX. Moreover, problem (20) is equivalent to [7, Eq. (18)], where an analytical expression for  $P'(r_E)$  was derived assuming a half-wave rectifier circuit with a single diode at the EH, a clipping model for the EH saturation, and perfect impedance matching. Thus, for this special case, (20), and hence, (9) yield the same solution as the one obtained in [7]. We note, however, that in this paper, we use a learning based model for  $P'(r_E)$ , which is applicable for imperfect impedance matching and arbitrary rectifier circuits.

### E. Learning Based Model For EH Circuits

In this section, we discuss a learning based approach to approximate functions  $f_v(v, r_E)$  and  $P'(v, r_E)$ , which are required for calculation of the transition pdf  $\rho_{i,j}(r_x)$  and the harvested power  $\tilde{P}_i(r_x)$  in optimization problems (9), (15), and (20).

As discussed in Section II-B, for practical EHs, given load voltage level,  $v$ , and the amplitude of the received symbol,  $r_E = |h_E|r_x$ , it is not tractable to develop exact analytical expressions of the transition function  $f_v(v, r_E)$  and the reward associated with the corresponding transition  $P'(\tilde{v}, r_E)$ , where  $\tilde{v}$  is the quantized voltage level  $v$ , because of the imperfections of the EH circuit. However, due to the universal approximation theorem for DNNs [31], it is possible to estimate the values of these functions with DNNs. To this end, we train two DNNs,  $\hat{f}_v(v, r_E) = \mathcal{N}_1(v, r_E, \Omega_1)$  and  $\hat{P}'(v, r_E) = \mathcal{N}_2(v, r_E, \Omega_2)$ , where  $\Omega_1$  and  $\Omega_2$  are the trainable parameters of the DNNs, and  $\hat{f}_v(v, r_E)$  and  $\hat{P}'(v, r_E)$  are the approximations of  $f_v(v, r_E)$  and  $P'(v, r_E)$ , respectively. Since the related approximation error depends on the network size [31], the numbers of nodes of DNNs  $\mathcal{N}_1$  and  $\mathcal{N}_2$  have to be chosen properly. For our simulations, we use DNNs where the hidden nodes employ ReLU activation functions. In the output layer, as the suitability of the logistic function for modeling saturation effects in EH circuits was demonstrated in [10], we use a sigmoid activation function [13].

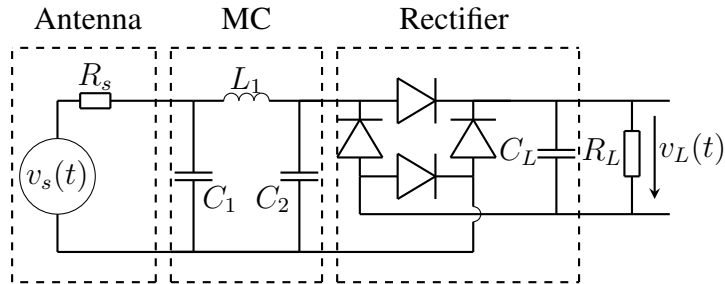


Fig. 4. EH circuit model comprising an MC, a full-wave rectifier based on the bridge diode configuration, and a capacitor  $C_L$  as part of an LPF.

In this paper, we consider two different rectenna EH circuits, namely, a single diode half-wave rectifier [7], cf. Fig. 3, and a bridge full-wave rectifier [23], cf. Fig. 4. For both rectenna circuits, we designed two different LC matching networks, fine-tuned for input signal frequency 2.45 GHz and input power values  $-13$  dBm and  $0$  dBm representing low and high input power levels, respectively. As discussed in Section II-B, although the MCs also include reactive elements, the memory introduced by the MC can be neglected in the MDP model since the MCs behave as band-pass filters, whose bandwidths are much larger than the considered symbol rates  $\frac{1}{T}$ , which do not exceed 200 kHz in our simulations. The adopted EH circuit parameters are specified in Table I.

Data for the training of the DNNs can be obtained from a circuit simulator, such as ADS [32]. To train the DNNs, we randomly generate the i.i.d. amplitudes of the received symbols,  $r_E$ , that are uniformly distributed over a space of symbols that can be realistically received by the EH and determine the corresponding 4-tuples  $\{P'(v_\nu, r_E), f_v(v_\nu, r_E), v_\nu, r_E\}$  using the circuit simulator. Specifically, we used 11000, 3000, and 750 4-tuples for training, validation, and testing of the DNNs for all considered circuits, respectively. For training, we used the Adam optimization algorithm [33] and the mean absolute percentage loss function, see e.g. [34].

To minimize the estimation error measured on the test set for a given training set size, we trained several DNNs with different numbers of layers to find the best setting. We found that, for all considered rectenna circuits, the values of the mean absolute percentage error for DNNs  $\mathcal{N}_1(v, r_E, \Omega_1)$  and  $\mathcal{N}_2(v, r_E, \Omega_2)$  do not significantly decrease if the size of the DNNs increases beyond 7 layers and 15 nodes per hidden layer. The parameters of each network obtained after training are saved to be used for estimation of the transition pdf  $\rho_{i,j}(r_x)$  and the power values

TABLE I  
EH CIRCUIT PARAMETERS.

Rectifier circuit	Half-wave rectifier		Full-wave rectifier	
Input power level for MC design	-13 dBm	0 dBm	-13 dBm	0 dBm
Diode model	SMS7630			
Antenna resistance	$R_s = 50 \Omega$			
Load capacitor	$C_L = 1 \text{ nF}$			
Load resistor	$R_L = 10 \text{ k}\Omega$			
Inductance of the MC	$L_1 = 26.7 \text{ nH}$	$L_1 = 9.62 \text{ nH}$	$L_1 = 23.2 \text{ nH}$	$L_1 = 11.1 \text{ nH}$
Capacitance of the MC	$C_1 = 0.73 \text{ pF}$	$C_1 = 1.41 \text{ pF}$	$C_1 = 0.3 \text{ pF}$	$C_1 = 2.72 \text{ pF}$
	-	$C_2 = 0.375 \text{ pF}$	-	$C_2 = 0.3 \text{ pF}$
3 dB bandwidth of the MC	270 MHz	280 MHz	310 MHz	300 MHz

$\tilde{P}_i(r_x)$ , respectively, as needed for solving optimization problems (9), (15), and (20).

#### IV. SIMULATION RESULTS

In this section, for convenience, we refer to the operational modes corresponding to the solutions of problems (9), (15), and (20) as Scheme I, Scheme II, and Scheme III, respectively. In the following, after specifying the simulation parameters, we first validate the proposed model by comparing the rate-power regions of the SWIPT system obtained for Schemes I-III with that obtained for the scheme proposed in [7]. Then, we investigate the impact of impedance mismatch between antenna and rectifier on the rate-power region. Subsequently, we study the dependence of the rate-power region on the symbol duration  $T$ , the type of EH circuit, and the EH input power level, respectively.

##### A. Simulation Parameters

For all simulations, we adopted uniformly spaced symbol amplitudes  $r_x$ , i.e.,  $r_{x_k} = \frac{k}{S-1} r_x^{\max}$ ,  $k = 0, 1, \dots, S-1$ , with maximum symbol amplitude  $r_x^{\max} = 10^{\frac{P_{\max}^{\text{TX}}}{20}}$ , where  $P_{\max}^{\text{TX}}$  is the PP limit at the TX in dBm and  $S$  is the constellation size. Furthermore, the IR and EH channel gains are modeled as  $h_l = \tilde{h}_l \left( \frac{c}{4\pi d_l f_c} \right)^{\alpha_l}$ ,  $l \in \{I, E\}$ , where  $\tilde{h}_l$  is the small scale fading coefficient, which is kept constant and equal to 1 unless specified otherwise,  $c$  denotes the speed of light,  $\alpha_l$  is the pathloss exponent, and  $d_I$  and  $d_E$  represent the distances between TX and IR and between TX and EH, respectively. Moreover, we consider three different input power regimes at

TABLE II  
SIMULATION PARAMETERS.

Parameter	Value
Carrier frequency	$f_c = 2.45$ GHz
PP limit at TX	$P_{\max}^{\text{TX}} = 50$ dBm
AP limit at TX	$\sigma_x^2 = 42$ dBm
Constellation size	$S = 64$
AWGN variance at IR	$\sigma_n^2 = -70$ dBm
Distance between TX and IR	$d_I = 40$ m
Pathloss exponent of IR channel	$\alpha_I = 3$
Distance between TX and EH	LP regime: $d_E = 20$ m MP regime: $d_E = 10$ m HP regime: $d_E = 2$ m
Pathloss exponent of EH channel	$\alpha_E = 2$
EH state space size	$S_{\Xi} = 50$
Maximum number of iterations of Algorithm 1	$M_{\max} = 15$ $N_{\max} = 10$
Initial tolerance in Algorithm 1	$\epsilon_1^{\text{tol}} = 0.5$
Tolerance decrease factor in Algorithm 1	$\delta_{\epsilon} = 0.5$

the EH, namely, the low power (LP), the medium power (MP), and the high power (HP) regimes characterized by different distances  $d_E$  between TX and EH. The adopted simulation parameters are summarized in Table II.

### B. Model Validation

In Fig. 5(a), for  $T = 100$   $\mu$ s, we compare the rate-power regions of the SWIPT system obtained for Schemes I-III and the baseline scheme from [7] in the LP and MP regimes. To this end, for all considered schemes, we show the expected mutual information  $\bar{I}(p_{r_x}^*)$  and the average harvested power  $\bar{P}(p_{r_x}^*)$  obtained with the circuit simulator ADS for the respective optimal input distribution  $p_{r_x}^*$ . We observe that, in the LP regime, all four schemes yield a similar performance since, in this case, the EH operates in the linear regime and the rectenna memory can be neglected because of the low input power and the large symbol duration, cf. Section III-D, respectively. However, in the MP regime, the saturation of the EH has an impact on performance. Thus, in this regime, the baseline scheme, which is based on an analytical model for the EH circuit, has

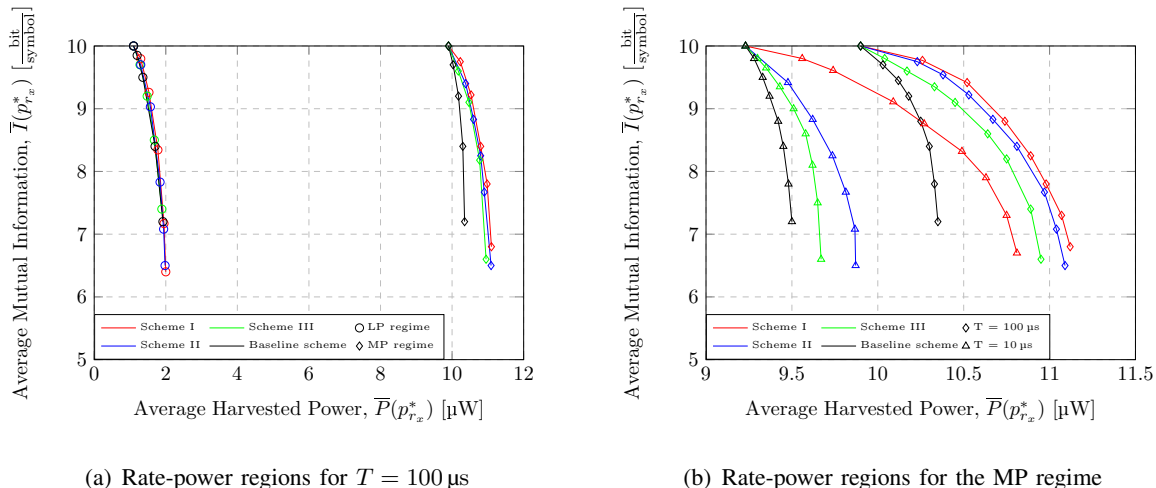


Fig. 5. Rate-power region for Schemes I, II, and III, and for the baseline scheme.

a worse performance than the other schemes, which employ a learning based model for the EH circuit and are able to better capture the impact of impedance mismatch and EH saturation.

In Fig. 5(b), for the MP regime, we compare the rate-power regions of the considered schemes for symbol durations  $T = 100 \mu s$  and  $T = 10 \mu s$ , respectively. We observe that, for all considered schemes, a shorter symbol duration generally leads to lower harvested powers. Furthermore, unlike for  $T = 100 \mu s$ , for  $T = 10 \mu s$ , there is a significant performance gap between Scheme I, for which the EH state is known at TX and IR, and the other schemes, for which the EH state is unknown at both devices. This is expected, since, for short  $T$ , the memory introduced by the EH is significant, which is exploited in Scheme I by finding the optimal input distribution for each EH state. In contrast, the other schemes have to find a compromise input distribution which yields a good performance for all the EH states. Additionally, we observe a larger performance gap between Schemes II and III for the shorter symbol duration since the EH memory is completely neglected in Scheme III. Finally, we note that, for a given symbol duration  $T$  and a given power regime, the input distributions and, hence, the harvested powers for all considered schemes are nearly identical for large  $\bar{I}(p_{r_x}^*)$  since, in this case, the solution of (9) is mainly determined by the feasible set specified by (9b) - (9f).

### C. Impact of Impedance Mismatch

In this section, we study the impact of impedance mismatch between antenna and rectifier on the performance of the SWIPT system. To this end, in Fig. 6, we show the rate-power regions

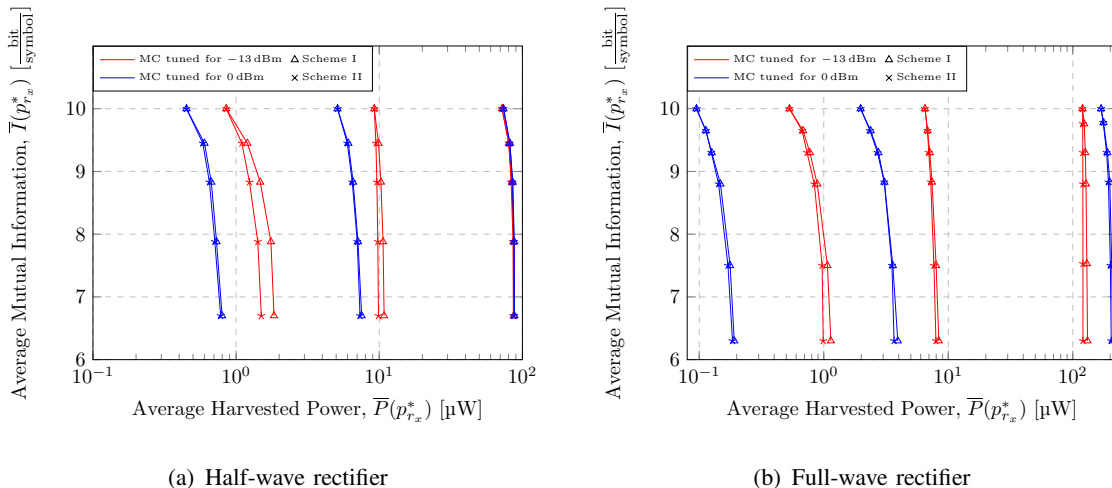


Fig. 6. Rate-power region for Schemes I and II for  $T = 10 \mu\text{s}$ .

for Schemes I and II for the LP, MP, and HP regimes. For the results shown in Fig. 6, we adopt a symbol duration of  $T = 10 \mu\text{s}$  and the MCs were tuned for two different input power levels, namely,  $-13 \text{ dBm}$  and  $0 \text{ dBm}$ . We show in Fig. 6(a) and Fig. 6(b) the rate-power regions obtained for half-wave and full-wave rectifiers, respectively.

We observe from Fig. 6 that, as expected, a larger input power generally leads to a higher average harvested power  $\bar{P}$ . Moreover, we note that, in the LP and MP regimes, for both rectifier circuits, the impedance mismatch caused by employing an MC fine-tuned for a relatively high input power level of  $0 \text{ dBm}$  yields a significant performance loss compared to an MC designed for a lower input power level of  $-13 \text{ dBm}$ . In contrast, in the HP regime, the MC tuned for  $0 \text{ dBm}$  outperforms the MC tuned for  $-13 \text{ dBm}$  for both rectifier circuits. However, the performance difference is much larger for the full-wave rectifier than for the half-wave rectifier. In fact, in the HP regime, the EH employing the half-wave rectifier is almost always driven into saturation which limits the amount of harvested power. Additionally, we note that, similar to Fig. 5, for a given rectifier circuit at the EH and a given input power regime, exploiting the knowledge of the EH state, i.e., Scheme I, typically yields a performance gain.

#### D. Influence of Symbol Duration and Input Power Regime

In this section, we study the impact of symbol duration  $T$  and the input power regime on the performance of Scheme II, i.e., when the EH state is not known at TX and IR. We assume that the EH is equipped with a half- or a full-wave rectifier and the impedance MC is designed for



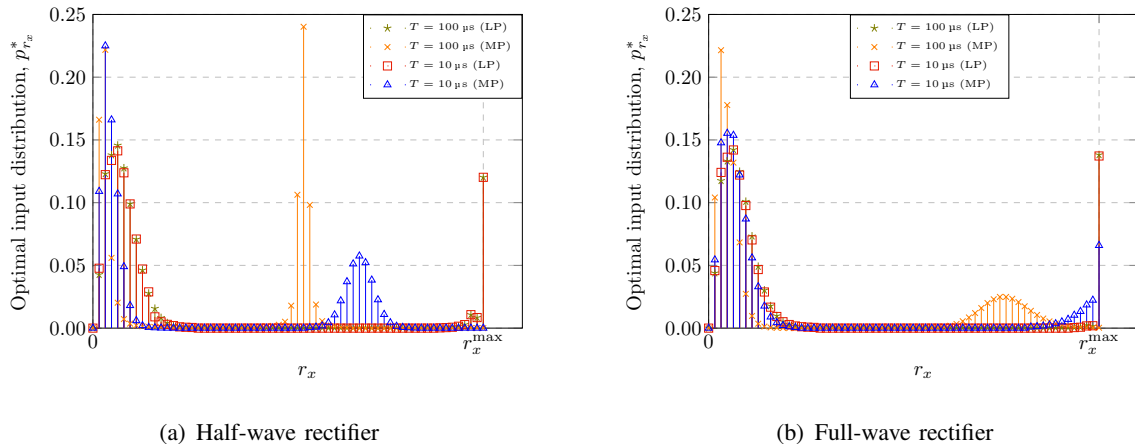


Fig. 7. Optimal input distribution for Scheme II with  $I_{\text{req}} = 6.5 \frac{\text{bit}}{\text{symbol}}$ .

the corresponding input power levels, i.e., the MCs are tuned for  $-13$  dBm in the LP and MP regimes and for  $0$  dBm in the HP regime, cf. Fig. 6.

In Fig. 7, we show the optimal distributions for Scheme II in the LP and MP regimes for symbol durations  $T = 100 \mu\text{s}$  and  $T = 10 \mu\text{s}$ . The required mutual information was set to  $I_{\text{req}} = 6.5 \frac{\text{bit}}{\text{symbol}}$ . We observe that, for both the half-wave rectifier (Fig. 7(a)) and the full-wave rectifier (Fig. 7(b)), the optimal input distribution is practically independent of symbol duration  $T$  in the LP regime, where it is optimal to allocate a probability of  $0.12$  and  $0.14$  to symbols having the maximum amplitude  $r_x^{\text{max}}$ , respectively, as even for this large amplitude, the EH circuit is not in saturation.

However, in the MP regime, for both symbol durations, the symbol amplitudes for the half-wave rectifier are limited to values smaller than  $r_x^{\text{max}}$  to avoid that the EH circuit is driven into saturation. Furthermore, the optimal input distribution depends on the value of the symbol duration. For short symbol durations, the capacitor  $C_L$  in the EH circuit cannot be fully charged within one symbol interval, and hence, larger symbol amplitudes can be afforded without driving the EH into saturation. Similarly, for the full-wave rectifier, in the MP regime, the optimal input distribution favors smaller amplitudes for  $T = 100 \mu\text{s}$ . However, the symbol amplitudes for the full-wave rectifier in the MP regime tend to be larger than those for the half-wave rectifier. This is due to the larger breakdown voltage of the former, where two identical diodes are connected in series, compared to the latter, which has only a single diode. Hence, in the MP regime, the optimal input distribution depends on the symbol duration and the rectifier circuit.

In Fig. 8, we show the boundaries of the rate-power region for Scheme II. Here, in order to

be able to illustrate the impact of the symbol duration on the data rate, we show the bit rate,  $R(p_{r_x}^*) = \frac{I(p_{r_x}^*)}{T}$ , as a function of the harvested power  $\bar{P}(p_{r_x}^*)$ . For the results shown in Fig. 8, we adopted Rayleigh fading for the IR channel, whereas, for the EH channel, we assumed a line of sight and, hence, Rician fading with Rician factor 1. The simulation results were averaged over 1000 channel realizations. In Fig. 8, the rate-power regions for different symbol durations and for the LP, MP, and HP regimes are depicted. First, similar to Fig. 6, we observe that, for both considered EH circuits and all considered symbol durations,  $T$ , higher input power levels lead to higher average harvested powers. Furthermore, for all considered symbol durations,  $T$ , the half-wave rectifier yields a better performance compared to the full-wave rectifier in the LP and MP regimes due to the smaller number of lossy non-linear diodes. However, in the HP regime, the full-wave rectifier performs better since the two diodes connected in series lead to a higher power saturation level. Furthermore, for all input power regimes and for both EH circuits, decreasing the symbol duration generally leads to an increase of the bit rate at the IR and a reduction of the average power that can be harvested by the EH. In particular, for the half-wave rectifier in the MP regime, average harvested power values larger than  $10 \mu\text{W}$  can be achieved only if the symbol duration exceeds  $T = 10 \mu\text{s}$ . Hence, Fig. 8 reveals that the rate-power region of the considered SWIPT system depends on the symbol duration, the input power level at the EH, and the type of EH circuit since the memory and non-linearity of the rectenna have a significant impact on the amount of harvested power.

## V. CONCLUSION

In this paper, we considered SWIPT systems that employ EHs with practical non-linear rectifier circuits with memory and impedance mismatch. We modeled the memory of the EH by an MDP and used DNNs to model the non-linear effects of the EH circuit. For optimization of the input symbol distribution, we considered the cases where TX and IR know and do not know the EH state. We showed that, for the optimal input symbol distribution, the phase of the transmit signal is independent of the signal amplitude and uniformly distributed. Furthermore, for the case where TX and IR know the instantaneous EH state, we formulated a convex optimization problem to determine the boundary of the rate-power region. Then, for the case where the EH state is not known at TX and IR, we showed that the corresponding optimization problem is non-convex and proposed an iterative algorithm based on alternating optimization to obtain a stationary point. In our simulation results, we considered EHs with half-wave and full-wave

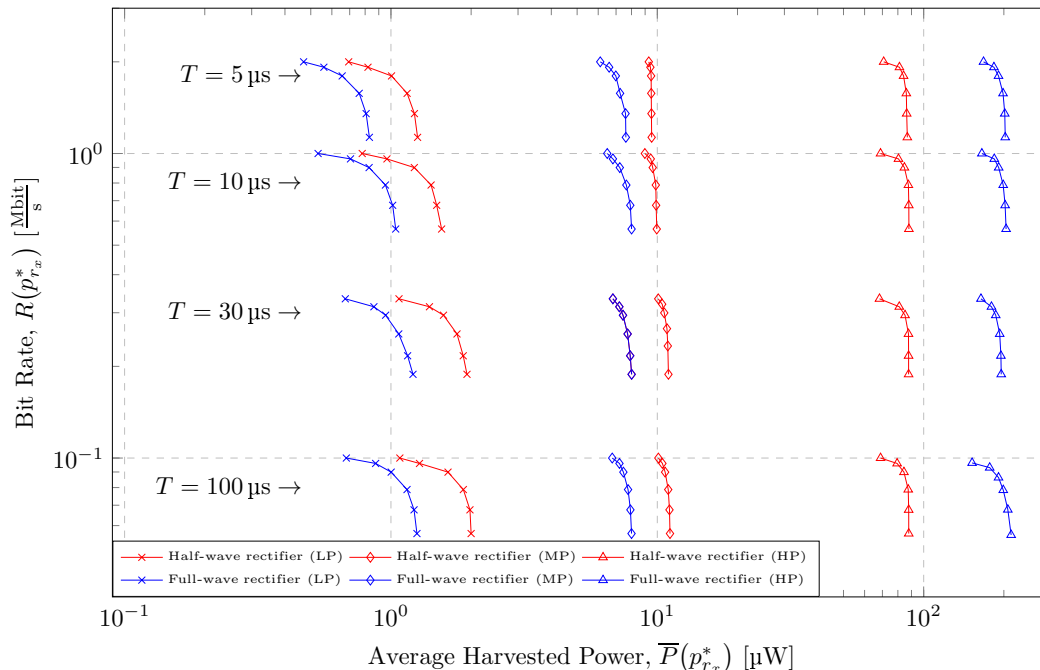


Fig. 8. Rate-power region for Scheme II, different symbol durations  $T$ , input power regimes, and rectifier circuits.

rectifier circuits. We validated our model by comparing it with a baseline scheme and studied the impact of the symbol duration, the EH input power level, the impedance mismatch between antenna and rectifier, and the type of EH circuit. We observed that, in the LP and MP regimes, the half-wave rectifier circuit yields a larger average harvested power than the full-wave rectifier, whereas, in the HP regime, the latter circuit significantly outperforms the former. Additionally, our results showed that, for both rectifier circuits and all considered input power regimes, a shorter symbol duration leads to a higher bit rate at the expense of a decrease of the average harvested power.

## APPENDIX A

### PROOF OF PROPOSITION 1

The following proof follows [28, Section II.B]. First, let us observe that for any concave function  $f(\cdot; \cdot)$ , and any  $F \in \mathbb{R}$ ,

$$\begin{aligned} \text{if } F \leq f(p_1; p_2) \leq f(p_1; p_2 = p'_2), \forall p_1, p_2, \\ \text{then } \{p_1 \mid f(p_1; p_2) \geq F\} \subseteq \{p_1 \mid f(p_1; p_2 = p'_2) \geq F\}, \end{aligned} \quad (21)$$

where  $p_1 \in \mathbb{P}_1$ ,  $p_2, p'_2 \in \mathbb{P}_2$ , and  $\mathbb{P}_1, \mathbb{P}_2$  are some sets of functions  $\mathbb{R} \mapsto \mathbb{R}$ .

Then, we note that the joint pdf of RVs  $r_y$  and  $\phi_y$  conditioned on  $r_x$  and  $\phi_x$  for the considered AWGN channel can be expressed as [28, Eq. (10)]

$$p_{r_y, \phi_y | r_x, \phi_x}(r_y, \phi_y | r_x, \phi_x) = \frac{r_y}{2\pi\sigma_n^2} e^{-\frac{r_y^2 + r_x^2 |h_I|^2 - 2r_x |h_I| r_y \cos(\phi_y - \phi_x - \phi_I)}{2\sigma_n^2}}. \quad (22)$$

Therefore, if the pdf of phase  $\phi_x \in (-\pi, \pi]$  is uniform and independent of  $r_x$ , then taking constraint (9d) into account, we obtain the marginal pdf  $p_{r_y}$  as a function of the input pdf  $p_{r_x}$  as follows

$$\begin{aligned} p_{r_y}(r_y; p_{r_x}) &= \int_0^{r_x^{\max}} \int_{-\pi}^{\pi} \int_{-\pi}^{\pi} p_{r_y, \phi_y | r_x, \phi_x}(r_y, \phi_y | r_x, \phi_x) \frac{1}{2\pi} p_{r_x}(r_x) d\phi_x d\phi_y dr_x \\ &= \frac{1}{\sigma_n^2} \int_0^{r_x^{\max}} r_y e^{-\frac{r_y^2 + r_x^2 |h_I|^2}{2\sigma_n^2}} I_0\left(\frac{r_y r_x |h_I|}{\sigma_n^2}\right) p_{r_x}(r_x) dr_x. \end{aligned} \quad (23)$$

Thus, if amplitude  $r_x$  and phase  $\phi_x$  are statistically independent and  $\phi_x$  is uniformly distributed, then amplitude  $r_y$  and phase  $\phi_y$  of the received signal are also mutually statistically independent. Moreover, in this case, the phase of the received signal is uniformly distributed and the pdf of the amplitude of the received signal,  $r_y$ , is given by (23).

Then, we note that the joint differential entropy of RVs  $r_y$  and  $\phi_y$  is always bounded as [28]  $H_{r_y, \phi_y} \leq H_{r_y} + \log_2(2\pi)$ , where  $H_{r_y}$  denotes the entropy of  $r_y$ . Moreover, the relation is satisfied with equality if  $\phi_y$  is uniformly distributed and independent of  $r_y$ , or equivalently, if  $\phi_x$  is uniformly distributed and independent of  $r_x$ .

Hence, for the mutual information achieved by input pdf  $p_{r_x, \phi_x}^i$ , we obtain

$$\begin{aligned} I(p_{r_x, \phi_x}^i) &= I(p_{r_x}^i, p_{\phi_x | r_x}^i) = H_{r_y, \phi_y}(p_{r_x, \phi_x}^i) + \int_0^\infty p_{r_y}(r_y; p_{r_x, \phi_x}^i) \log_2(r_y) dr_y - H_n \\ &\leq I(p_{r_x}^i, p_{\phi_x | r_x}^i = p_{\phi_x}^{\text{uni}}) = H_{r_y}(p_{r_x}^i) + \int_0^\infty p_{r_y}(r_y; p_{r_x}^i) \log_2(r_y) dr_y + \log_2(2\pi) - H_n, \end{aligned} \quad (24)$$

where  $p_{\phi_x}^{\text{uni}}$  denotes the uniform pdf of  $\phi_x$ . In (24), equality holds if  $r_x$  and  $\phi_x$  are independent,  $\phi_x$  is uniformly distributed and, hence, is independent of EH state  $\xi$ .

Furthermore, we note that the average mutual information  $\bar{I}$  in (9b) is defined as a weighted sum of the individual values  $I(p_{r_x, \phi_x}^i)$ , i.e.,  $\bar{I}(\boldsymbol{\pi}(r_x), \mathcal{P}_{\phi_x | r_x}) = \sum_{i=1}^{S_\Xi} \gamma_i I(p_{r_x, \phi_x}^i)$ . Hence, we can rewrite constraint (9b) as follows

$$I_{\text{req}} \leq \bar{I}(\boldsymbol{\pi}(r_x), \mathcal{P}_{\phi_x | r_x}) = \sum_{i=1}^{S_\Xi} \gamma_i I(p_{r_x, \phi_x}^i) \leq \sum_{i=1}^{S_\Xi} \gamma_i I(p_{r_x}^i, p_{\phi_x | r_x}^i = p_{\phi_x}^{\text{uni}}) = \bar{I}(\boldsymbol{\pi}(r_x)). \quad (25)$$

Since  $I(\cdot, \cdot)$  and, hence,  $\bar{I}(\cdot, \cdot)$  in (25) are concave, then, from (21),

$$\{\boldsymbol{\pi}(r_x) \mid \bar{I}(\boldsymbol{\pi}(r_x), \mathcal{P}_{\phi_x | r_x}) \geq I_{\text{req}}\} \subseteq \{\boldsymbol{\pi}(r_x) \mid \bar{I}(\boldsymbol{\pi}(r_x); p_{\phi_x | r_x}^i = p_{\phi_x}^{\text{uni}}) \geq I_{\text{req}}\}. \quad (26)$$

Thus, independently distributed RVs  $r_y$  and  $\phi_y$  with uniformly distributed  $\phi_y$  lead to the largest set of pdfs  $\pi(r_x)$  with  $\bar{I}(\pi(r_x), \mathcal{P}_{\phi_x|r_x}) \geq I_{\text{req}}$ . Since the objective function and the other constraints in (9) do not depend on  $\mathcal{P}_{\phi_x|r_x}$ , this condition also leads to the largest feasible set of pdfs  $\pi(r_x)$  for optimization problem (9). Therefore, for the optimal solution of (9), the phase  $\phi_x$  is uniformly distributed and statistically independent of the state  $\xi$  and the amplitude  $r_x$ . Moreover, the marginal pdf of the output symbol amplitudes,  $p_{r_y}(r_y; p_{r_x})$ , is given by (23), whereas the mutual information in (24) can be simplified to the expression in (10) This completes the proof.

## REFERENCES

- [1] N. Shanin, L. Cottatellucci, and R. Schober, "Rate-power region of SWIPT systems employing nonlinear energy harvester circuits with memory," in *Proc. IEEE Int. Conf. Commun. (ICC)*, 2020.
- [2] B. Clerckx, R. Zhang, R. Schober, D. W. K. Ng, D. I. Kim, and H. V. Poor, "Fundamentals of wireless information and power transfer: From RF energy harvester models to signal and system designs," *IEEE J. Sel. Areas Commun.*, vol. 37, no. 1, pp. 4–33, Jan. 2019.
- [3] L. R. Varshney, "Transporting information and energy simultaneously," in *Proc. IEEE Int. Symp. Information Theory*, Jul. 2008, pp. 1612–1616.
- [4] P. Grover and A. Sahai, "Shannon meets Tesla: Wireless information and power transfer," in *Proc. IEEE Int. Symp. Information Theory*, Jun. 2010, pp. 2363–2367.
- [5] R. Zhang and C. K. Ho, "MIMO broadcasting for simultaneous wireless information and power transfer," *IEEE Trans. Wirel. Commun.*, vol. 12, no. 5, pp. 1989–2001, May 2013.
- [6] B. Clerckx, "Wireless information and power transfer: Nonlinearity, waveform design, and rate-energy tradeoff," *IEEE Trans. Signal Process.*, vol. 66, no. 4, pp. 847–862, Feb. 2018.
- [7] R. Morsi, V. Jamali, A. Hagelauer, D. W. K. Ng, and R. Schober, "Conditional capacity and transmit signal design for SWIPT systems with multiple nonlinear energy harvesting receivers," *IEEE Trans. Commun.*, vol. 68, no. 1, pp. 582–601, Jan. 2020.
- [8] A. Collado and A. Georgiadis, "Optimal waveforms for efficient wireless power transmission," *IEEE Microw. Wirel. Compon. Lett.*, vol. 24, no. 5, pp. 354–356, May 2014.
- [9] E. Boshkovska, A. Koelpin, D. W. K. Ng, N. Zlatanov, and R. Schober, "Robust beamforming for SWIPT systems with nonlinear energy harvesting model," in *Proc. IEEE 17th Int. Workshop Signal Processing Advances in Wireless Communications (SPAWC)*, Jul. 2016, pp. 1–5.
- [10] E. Boshkovska, D. W. K. Ng, N. Zlatanov, and R. Schober, "Practical non-linear energy harvesting model and resource allocation for SWIPT systems," *IEEE Commun. Lett.*, vol. 19, no. 12, pp. 2082–2085, Dec. 2015.
- [11] M. Varasteh, E. Piovano, and B. Clerckx, "A learning approach to wireless information and power transfer signal and system design," in *Proc. Speech and Signal Processing (ICASSP)*, May 2019, pp. 4534–4538.
- [12] M. Varasteh, J. Hoydis, and B. Clerckx, "Learning modulation design for SWIPT with nonlinear energy harvester: Large and small signal power regimes," in *Proc. IEEE 20th Int. Workshop Signal Processing Advances in Wireless Commun. (SPAWC)*, Jul. 2019, pp. 1–5.

- [13] I. Goodfellow, Y. Bengio, and A. Courville, *Deep Learning*. MIT Press, 2016.
- [14] P. Horowitz and W. Hill, *The Art of Electronics*, 2nd ed. Cambridge University Press, 1989.
- [15] P. S. Heljo, M. Li, K. E. Lilja, H. S. Majumdar, and D. Lupo, "Printed half-wave and full-wave rectifier circuits based on organic diodes," *IEEE Trans. Electron Devices*, vol. 60, no. 2, pp. 870–874, Feb. 2013.
- [16] E. Altman, *Constrained Markov Decision Processes*. CRC Press, 1999, vol. 7.
- [17] J. C. Bezdek and R. J. Hathaway, "Some notes on alternating optimization," in *AFSS Int. Conf. on Fuzzy Systems*. Springer, 2002, pp. 288–300.
- [18] L. Grippo and M. Sciandrone, "On the convergence of the block nonlinear Gauss-Seidel method under convex constraints," *Operations research letters*, vol. 26, no. 3, pp. 127–136, 2000.
- [19] X. Yu, D. Xu, Y. Sun, D. W. K. Ng, and R. Schober, "Robust and secure wireless communications via intelligent reflecting surfaces," *arXiv preprint arXiv:1912.01497*, 2019.
- [20] X. Le Polozec, "A simple formula to calculate the diode junction resistance variations with RF power of a series Schottky diode detector," 2016, DOI: 10.13140/RG.2.2.27882.31681.
- [21] J. Guo, H. Zhang, and X. Zhu, "Theoretical analysis of RF-DC conversion efficiency for Class-F rectifiers," *IEEE Trans. Microw. Theory Tech.*, vol. 62, no. 4, pp. 977–985, Apr. 2014.
- [22] Z. Feng, R. Dearden, N. Meuleau, and R. Washington, "Dynamic programming for structured continuous Markov Decision Problems," in *Proc. of the 20th Conf. on Uncertainty in Artificial Intelligence*, 2004.
- [23] U. Tietze and C. Schenk, *Advanced Electronic Circuits*. Springer Science & Business Media, 2012.
- [24] J. R. Norris, *Markov Chains*. Cambridge University Press, 1998.
- [25] S. P. Meyn and R. L. Tweedie, *Markov Chains and Stochastic Stability*. Springer Science & Business Media, 2012.
- [26] J. G. Smith, "The information capacity of amplitude- and variance-constrained scalar Gaussian channels," *Inf. and Control*, vol. 18, 1971.
- [27] D. Tse and P. Viswanath, *Fundamentals of Wireless Communication*. Cambridge University Press, 2005.
- [28] S. Shamai and I. Bar-David, "The capacity of average and peak-power-limited quadrature Gaussian channels," *IEEE Trans. Inf. Theory*, vol. 41, no. 4, pp. 1060–1071, 1995.
- [29] M. Grant and S. Boyd, "CVX: Matlab software for disciplined convex programming, version 2.0 beta (2013)," URL: <http://cvxr.com/cvx>, 2015.
- [30] C. Si, J. An, T. Lan, T. Ußmüller, L. Wang, and Q. Wu, "On the equality constraints tolerance of constrained optimization problems," *Theor. Comput. Sci.*, vol. 551, pp. 55–65, 2014.
- [31] B. Hanin, "Universal function approximation by deep neural nets with bounded width and ReLU activations," *arXiv preprint arXiv:1708.02691*, 2017.
- [32] The Keysight Technologies, Inc., *Electronic Design Automation (EDA) Software, Advanced Design System (ADS), Version 2017*.
- [33] D. P. Kingma and J. Ba, "Adam: A method for stochastic optimization," in *Proc. of the 3rd Int. Conf. on Learning Representations (ICLR)*, 2015.
- [34] A. D. Myttenaere, B. Golden, B. L. Grand, and F. Rossi, "Mean absolute percentage error for regression models," *Neurocomputing, Elsevier - Selected papers from the ESANN 2015*, vol. 192, pp. 38–48, 2016.